Nano Energy 122 (2024) 109286

Contents lists available at ScienceDirect

Nano Energy

journal homepage: www.elsevier.com/locate/nanoen

Full paper

A green approach to induce and steer chemical reactions using inert solid dielectrics☆

Shaoxin Li [a,b], Zhiwei Zhang [a,b], Puguang Peng [a,b], Xiang Li [a,b], Zhong Lin Wang [a,c,*], Di Wei [a,*]

[a] Beijing Institute of Nanoenergy and Nanosystems, Chinese Academy of Sciences, Beijing 101400, PR China
[b] School of Nanoscience and Engineering, University of Chinese Academy of Sciences, Beijing 100049, PR China
[c] Georgia Institute of Technology, Atlanta, GA 30332, USA

ARTICLE INFO

Keywords:
Contact electrification
Solid dielectrics
Contact-electro-chemistry
Electron transfer
Radical generation

ABSTRACT

The solid-liquid interface plays pivotal role in chemical reactions, but the contact electrification (CE) at interface is usually overlooked. Recently the CE effect was reported to promote interfacial chemistry as well as catalysis for organic pollutants. However, the exact role of CE in various chemical reactions remained unclear, and understanding of its influences has been a long-lasting challenge. Here, we proposed a paradigm of contact-electrochemistry (CE-Chemistry) via CE between solid dielectrics and liquids to show how their physical contact can induce and even guide reactions. CE-Chemistry was proved to exist ubiquitously in various reactions within both aqueous and non-aqueous systems, including redox reactions, organic polymerizations, pollutant degradations etc. The trade-off between electron transfer and ion migration at the solid dielectrics and liquids interface was elucidated to optimize reactions. Furthermore, a guidance that unified the concept of work functions, electronegativity in triboelectric series and standard electrode potentials was developed based on the electron transfer capabilities to steer reactions and assess their extent. This work not only reveals the physicochemical essence of CE, but also offers a new perspective to investigate the interface interaction across interdisciplinary subjects of physics, chemistry and material science.

1. Introduction

Vast majority of chemical reactions in industry and labs are performed in solutions, relying on initiators or external electric field to promote the generation of end products. Initiators are widely used in the chemical reactions, but they are inevitable to bring the complex product purification process and the consequent pollution [1]. On the other hand, electrochemical reaction is constrained by the limited choice of electroactive material and electrochemical windows when applying external electric field [2]. As such, pursuing a green, simple and universal protocol to induce chemical reactions is desperately needed. Mechanochemistry refers to mechanically activated chemistry through ball mill, planetary mill reactors or in twin-screw extruders etc. It offers unique benefit to initiate chemical reactions and ameliorate the pollution challenge of organic synthesis [3]. Mechanochemical reactions could be generally promoted by liquid-assisted grinding, in which the defects of materials, local high temperature/pressure conditions, and bond breaking/forming induced by the mechanical force effects had been extensively investigated [4–7]. However, little attention has been paid to the potential contributions made by solid-liquid contact electrification (CE), which commonly occurred in the form of frequent contact and separation during the mechanochemical processes.

Solid dielectrics with extremely inert chemical activity, such as fluorinated ethylene propylene (FEP) and polytetrafluoroethylene (PTFE), could reduce metal cations (e.g. Cu^{2+}, Au^{+}, Ag^{+}, Pb^{+}) in solution after triboelectrically charged by CE, which demonstrated the critical role of CE in chemical reactions [8,9]. These electrostatic charges on the solid dielectric surface were thought to be excess electrons developed during CE and their subsequent transfer to the reactants in the solution. However, some other studies revealed the chemical reactions might be driven by radicals created during CE [10–12]. These results indicated CE process between the inert dielectrics and liquids is

☆ Prof Zhong Lin Wang, an author on this paper, is the Editor-in-Chief of Nano Energy, but he had no involvement in the peer review process used to assess this work submitted to Nano Energy. This paper was assessed, and the corresponding peer review managed by Professor Chenguo Hu, also an Associate Editor in Nano Energy

* Corresponding authors at: Beijing Institute of Nanoenergy and Nanosystems, Chinese Academy of Sciences, Beijing 101400, PR China.
E-mail addresses: zhong.wang@mse.gatech.edu (Z.L. Wang), weidi@binn.cas.cn (D. Wei).

https://doi.org/10.1016/j.nanoen.2024.109286
Received 28 November 2023; Received in revised form 9 January 2024; Accepted 10 January 2024
Available online 13 January 2024

not a simple physical charge transfer, but involves contact-electro-catalytic reactions, for example, the metal leaching, the degradation of organic pollutants and the generation of H_2O_2 [13–15]. Such contact-electro-catalysis provides a new paradigm in the area of metal-free catalysis. It is also intrinsically different from the piezoelectric mechanocatalysis, in which the reaction relies on the piezoelectric materials [16]. However, reactions should not be limited to catalysis alone and exploration of various CE induced chemical reactions has not been reported. It should be noted that the electric double layer (EDL) at the interface of solid dielectrics and liquids will be formed by the synergistic effect of electron transfer and ion migration [17,18]. The influence of EDL on the CE induced chemical reactions is still unclear.

As the CE process is steerable and closely related to the electronegativity of the solid dielectrics [19], it may provide a scheme to steer chemical reactions and a reliable platform to investigate interactions between the solid dielectrics and liquids. Here, a comprehensive paradigm of contact-electro-chemistry (CE-Chemistry) was proposed, in which chemical reactions were proved to be initiated by the radicals generated during CE process at the solid dielectric-liquid interface. The CE-Chemistry was shown to cover a broad field in the subject of chemistry, including contact-electro-redox (CE-Redox) reaction of $[Fe(CN)_6]^{3-}$/$[Fe(CN)_6]^{4-}$, contact-electro-Polymerization (CE-Polymerization) of aniline, contact-electro-Catalysis (CE-Catalysis) of phenol and contact-electro-Fluorescence (CE-Fluorescence) of terephthalic acid (THA), etc. The role of EDL formation in the aqueous system was explored to balance the electronic-ionic transfer relationship and optimize the CE-Chemical reactions. In addition, the CE-Chemistry was performed for the first time in the non-aqueous system, which further revealed the ubiquity of the CE-Chemical mechanism beyond the aqueous system. Generally, the electron-accepting/donating capability of solid dielectrics during CE is closely related to their own electronegativity property, which depends on the electron affinity on the atoms of their chemical structure, and analogous to the electronic theory from Lewis acid-base law in chemistry. Combined with work function of the charge collector and standard electrode potentials of the electroactive species in the liquid, the electronegativity in triboelectric series of the solid dielectrics might be served as a benchmark to forecast the thermodynamics of CE-Chemical reactions. Therefore, a guidance that unified the concept of the work function, the electronegativity in triboelectric series, and the standard electrode potentials was proposed to steer chemical reactions and assess their extent. Different from chemical reactions initiated by light, heat, electricity, or chemicals etc., the CE-Chemistry based on the mechanical contact-separation method opens up a new avenue to investigate the interface interaction across multidisciplinary subjects of physics, material science, and chemistry.

2. Results

2.1. CE-Chemistry

CE is a ubiquitous phenomenon in our daily life where two surfaces get electrically charged once they contact with each other [20]. As shown in Figure S1a and S1b, the deionized (DI) water droplet was positively charged to about 0.6 nC after contacting the hydrophobic FEP film (contact angle of 101.99°), which corresponded to +1.5 V that was calculated by the formulation $V = \frac{Q}{C}$, where the capacitance of the Faraday cup was measured to be about 0.4 nF. In contrast, the surface potential of FEP changed from −1.1 V to −11.7 V (Figure S1c) after several DI water droplets moving away, which showed the DI water droplet and FEP film would be oppositely charged during CE. Moreover, the accumulation of transferred charge was observed through immersing repeatedly single electrode triboelectric nanogenerator (SE-TENG) mainly made of FEP into DI water (Figure S2a and Figure S2b), and its details were shown in Figure S3. These results indicated that the multiple contact-separation cycles could promote the amount of interfacial transferred charge between FEP and water. Herein, those CE effects have also been revealed in CE-Chemistry. Specifically, 0.01 mM potassium chloride (KCl) solution, 0.20 mM potassium ferrocyanide ($K_4[Fe(CN)_6]$) solution, and the dielectric FEP film were chosen to promote the CE-Oxidation of $[Fe(CN)_6]^{4-}$ to $[Fe(CN)_6]^{3-}$. The design of the experiment was illustrated in Fig. 1a, FEP film was firstly cut into pieces (about 1.0 cm × 1.5 cm each piece), and then the shredded FEP films were put into the aqueous solution containing 0.01 mM KCl and 0.20 mM $K_4[Fe(CN)_6]$. Ultrasonication (US) was used to create frequent contact-separation cycles at the solid dielectric-water interface due to continual cavitation bubble collapses [21]. To clarify the specific role of US in chemical reactions, in situ ultrasonic-electrochemical technique was used for voltametric studies (Figure S4(a)) with glassy carbon as the working electrode (diameter: 3.0 mm), platinum plate (size: 0.5 cm × 1.0 cm) as counter electrode and Ag/AgCl as the reference electrode. The cyclic voltammogram (CV) of $[Fe(CN)_6]^{4-}$ without (w/o) and with (w) US were shown in Figure S4(b). W/o the US, the CV scan curve showed a pair of redox peaks that represented the electron-transfer and mass diffusion controlled processes at the surface of electrode. In contrast, a plateau appeared in the CV scan curve under US when the external voltage exceeded 0.36 V, which indicated a highly effective mass transfer was realized by the bubble cavitation during US to enable an efficient electron-transfer controlled reaction process. Each pulse current peak was a consequence of an individual collapse of a cavitation bubble that took place near the electrode surface [22], indicating a dynamic process of contact-separation at solid-liquid interface. Electrochemical impedance spectroscopy (EIS) showed a decrease in the charge transfer resistance (R_{ct}) under US compared to that w/o US, as shown in the Nyquist plot in Figure S4(c). The equivalent circuit was depicted in Figure S4(d), in which R_p was the polarization resistance, CPE1 and CPE2 were the constant phase elements, W_o was the Warburg impedance. These results indicated US could be served to thin the diffusion layer and enhance mass transfer in solution [23]. Furthermore, the advantage of US was also be proved at 25 μm glass-encased Pt ultramicroelectrode as working electrode, as shown in figure S5, the oxidation current and R_{ct} of $[Fe(CN)_6]^{4-}$ under US is lager and lower than that w/o US. Therefore, US with a frequency of 40 kHz and a power of 420 W was employed here to mimic high-frequency contact-separation cycles between solid dielectrics and liquids with sufficient charge transfer and improve mass transfer in solution. It can be seen from Fig. 1b and Figure S6 that the color of original reduced $K_4[Fe(CN)_6]$ solution changed from transparent to light green after US in the presence of shredded FEP films for 12 h. Ultraviolet-Visible (UV-Vis) spectroscopy was used to investigate the coloration process, and its results showed that the characteristic absorption peak of the oxidized $K_3[Fe(CN)_6]$ at 260.0 nm, 303.0 nm, 325.0 nm, 421.0 nm [24] increased as the US time growth (Fig. 1c). To further identify the oxidized $K_3[Fe(CN)_6]$ generated during CE, the CV scan of the solution before and after US was measured by electrochemical methods (Fig. 1d). Before the US, the original solution contained only reduced $K_4[Fe(CN)_6]$ and had no reduction peak in the first CV scan from high potential to low potential. In contrast, after US for the original solution with shredded FEP films, the reduction characteristic peak in the first CV scan corresponding to the existence of $K_3[Fe(CN)_6]$ appeared, which indicated the CE-Oxidation of $[Fe(CN)_6]^{4-}$ to $[Fe(CN)_6]^{3-}$. Both of their second CV scan showed similar redox peaks because both the $[Fe(CN)_6]^{4-}$ and $[Fe(CN)_6]^{3-}$ co-existed in the solution at this time. Under the same time of US with reduced $K_4[Fe(CN)_6]$ solution, controlled experiment was conducted in absence of FEP (Figure S7). W/o FEP, neither the obvious increase in UV-Vis absorption peaks at 260.0 nm, 303.0 nm, 421.0 nm nor the significant reduction current peak in the first CV scan appeared, which suggested that FEP was essential to enhance the CE-Oxidation of $K_4[Fe(CN)_6]$.

It is well known that solid dielectrics with discrepant electronegativity would cause differences in their CE performance. It had been reported that the more fluorine groups in solid dielectrics, the stronger its electron-accepting capability [25]. Figure S8(a), figure S9(a) and figure

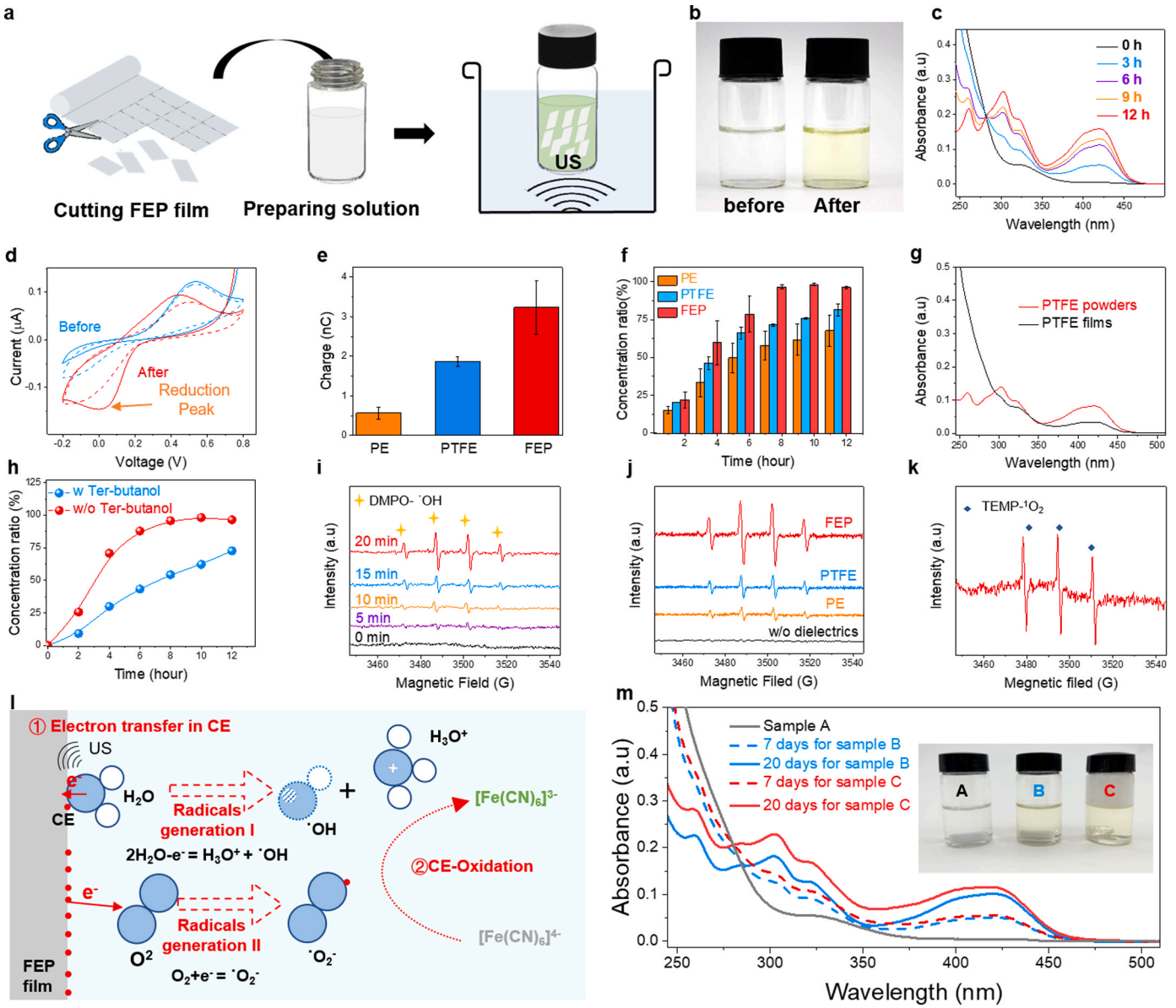

Fig. 1. CE-Chemistry. (a) Schematic of CE-Chemical experimental process. (b) Photograph of 0.20 mM $K_4[Fe(CN)_6]$ and 0.01 mM KCl solution (12 mL) before and after US for 12 h with shredded FEP film (thickness: 30 μm, total area: 600 cm^2). (c) UV-Vis spectra of reduced $K_4[Fe(CN)_6]$ solution during US in the presence of shredded FEP film for 12 h. (d) CV scan curve (scan rate: 1 mV/s) of reduced $K_4[Fe(CN)_6]$ solution before (blue line) and after (red line) US in the presence of shredded FEP film, the solid and dashed lines are the first and second CV scan cycle, respectively. (e) Concentration ratio of product ($K_3[Fe(CN)_6]$) in reduced $K_4[Fe(CN)_6]$ solution after US in the presence of different solid dielectrics. (f) Charge transfer during different solid dielectric-liquid CE. (g) UV-Vis spectra of reduced $K_4[Fe(CN)_6]$ solution during CE-Chemistry with PTFE powders and shredded PTFE films. (h) Concentration ratio of product ($K_3[Fe(CN)_6]$) after reduced $K_4[Fe(CN)_6]$ solution US w and w/o 1.00 M Ter-butanol. (i) Measured EPR spectra intensity in DI water with FEP under various US time. (j) Measured EPR intensity of ˙OH radicals generated by various solid dielectrics in DI water in contrast with the one w/o solid dielectrics. (k) Measured $^1O_2$ in DI water in the presence of FEP films. (l) Working mechanism of CE-Oxidation reaction of $[Fe(CN)_6]^{4-}$ to $[Fe(CN)_6]^{3-}$. (m) Photograph and UV-Vis spectra of reduced $K_4[Fe(CN)_6]$ solution under different conditions, in which sample A is the original 0.20 mM $K_4[Fe(CN)_6]$ and 0.01 mM KCl solution with quiescent PTFE stir bar, sample B is the original solution with rotating PTFE stir bar, sample C is the original solution with rotating PTFE stir bar and 0.20 g PTFE powders.

S10(a) depicted the chemical structure of FEP, PTFE and PE, respectively. As depicted in Fig. 1e, the tendency of CE performance between PE/PTFE/FEP and aqueous solutions was increased in sequence. Additionally, the yield of product (oxidized $K_3[Fe(CN)_6]$) during CE-Oxidation in the presence of shredded solid dielectrics followed the same trend of PE < PTFE < FEP, which might be closely related to the electron-accepting capability of solid dielectrics. Thus, it provided a new and straightforward way to steer the chemical reactions by choosing the optimized solid dielectric material in CE-Chemistry. Both microscopic pictures, X-ray diffraction (XRD), X-ray photoelectron spectrometer (XPS) spectra of the dielectrics before and after CE-Oxidation (Figures S8, S9, and S10) showed neither changes in morphology nor chemical composition. These results exhibited the unique advantages of sustainability when the inert solid dielectrics were used in CE-Chemical reactions. Besides, the smaller size of solid dielectric promoted the yield of product (oxidized $K_3[Fe(CN)_6]$), as shown in figure S11. This was due to the reason that the specific surface area of the FEP was increased when they were shredded into smaller pieces to increase the contact electrification area of the solid-liquid interface, promoting the CE-Chemistry. Furthermore, in the reduced $K_4[Fe(CN)_6]$ solution with very small amount of PTFE powders (0.2 g), after CE-Oxidation, the products (oxidized $K_3[Fe(CN)_6]$) yield was even higher than that with

the shredded PTFE films (4.0 g) (Fig. 1g). To further understand the underlying mechanism of CE-Chemistry, 1.00 M tert-butanol that is a common hydroxyl radical (·OH) scavenger was added in the solution containing only the reduced $K_4[Fe(CN)_6]$. As depicted in Fig. 1h, the yield of oxidized $K_3[Fe(CN)_6]$ in $K_4[Fe(CN)_6]$ solution with tert-butanol almost was halved (decreased from 95.7% to 54.3%) compared with that of original solution under the same US time of 8 h, which indicated that the ·OH radicals played an important role in CE-Oxidation of $[Fe(CN)_6]^{4-}$ to $[Fe(CN)_6]^{3-}$. The production of ·OH radicals during the CE process between FEP and DI water was detected by electron paramagnetic resonance (EPR) spectroscopy, in which 0.10 M 5,5-dimethyl-1-pyrroline N-oxide (DMPO) was used as ·OH radicals capturing agent. It can be seen from Fig. 1i that the quadruplet characteristic peaks of DMPO-·OH became stronger with increase in US time, which indicated that continues CE process could facilitate the yield of ·OH radicals. The change in EPR intensity of ·OH radicals in DI water during US in the pure DI water and in the presence of various solid dielectrics indicated that the CE-Chemical process was realized with radicals as intermediates and solid dielectrics played an important role to affect the radical production (Fig. 1j). On the other hand, the ambient air contains oxygen (O_2), and the dissolved O_2 could also facilitate the CE-Chemical reactions [14]. Figure S12 showed that the yield of oxidized $K_3[Fe(CN)_6]$ decreased when the solution was purged with nitrogen (N_2). This is possibly because O_2 captured the electron from the FEP-water interface to generate the superoxide radicals ($\cdot O_2^-$) in the solution to promote the oxidation reaction of $K_4[Fe(CN)_6]$. Here, the singlet oxygen ($^1O_2$) was detected by 0.10 M 2,2,6,6-tetramethyl-4-piperidone (TEMP) during the DI water US in the presence of FEP, as shown in Fig. 1k. It is generally believed that $^1O_2$ is the product of the oxidation by the $\cdot O_2^-$ radicals [26], thus it proved the existence of the $\cdot O_2^-$ radicals in the CE-Oxidation. Therefore, the mechanism of the CE-Oxidation of $[Fe(CN)_6]^{4-}$ to $[Fe(CN)_6]^{3-}$ was illustrated step-by-step in Fig. 1l. Frequent CE at the FEP-water interface might be induced by the collapse of cavitation bubbles under US, where electron transfer from water to FEP resulted in the formation of hydronium cations and ·OH radicals. Meanwhile, the O_2 dissolved in the solution could capture the electron from the charged FEP surface to form $\cdot O_2^-$ radicals. Thus, the reduced $[Fe(CN)_6]^{4-}$ in solution could be oxidized to $[Fe(CN)_6]^{3-}$ thanks to the oxidative characteristics of ·OH radicals and $\cdot O_2^-$ radicals.

In addition, we found the CE-Oxidation could be also realized through mechanical stirring w/o US. As depicted in Fig. 1m, nothing had been observed in sample A (0.20 mM $K_4[Fe(CN)_6]$, 0.01 mM KCl and PTFE stir bar) w/o any external mechanical stimulation. On the contrary, the solution color of sample B (0.20 mM $K_4[Fe(CN)_6]$, 0.01 mM KCl and PTFE stir bar) and sample C (0.20 mM $K_4[Fe(CN)_6]$, 0.01 mM KCl, PTFE stir bar, and 0.20 g PTFE powders) both turned from transparent to green after stirring (rotating speed:1500 rpm) 7 days and 20 days. The UV-Vis plot indicated that prolonging the mechanical force time or increasing the contact area of solid dielectric-water could effectively promote the reaction process of the CE-Oxidation. These results suggested that the long-term stirring force could induce CE-Chemical reactions even w/o US. This further showed that the CE-Chemistry dose not rely on the US and can be distinguished from the traditional sonochemistry. The main function of US here might be to enhance contact-separation cycles and contact forces between solid dielectrics and liquids. Furthermore, the CE-Fluorescence was also achieved by introducing the shredded FEP films into the terephthalic acid (THA) solution under US. As depicted in Figure S13a, the emission fluorescence intensity of THA-·OH products (425.0 nm) increased gradually with the increase in US time. The fluorescence process in the presence of different solid dielectrics after US was shown in Figure S13b, and the possible reaction pathway was shown in figure S13c. This further demonstrated the universality of CE-Chemical method, and indicated the important role of electronegativity of dielectrics in steering chemical reactions.

2.2. CE-Chemistry in organic reaction

Radicals are known to be highly reactive and play an important role in organic reactions. Accordingly, the CE-Chemical method should be also suitable to induce a series of organic reactions, for example, organic polymerization or catalytic degradation. Here, the CE-Polymerization was demonstrated as an effective way to synthesize organic polymers. As shown in Fig. 2a, the color of the aniline monomer solution (0.50 M aniline and 0.50 M H_2SO_4 in DI water) turned from light yellow to brown after US in the presence of shredded FEP films for 10 h. More obvious color contrast of the solution before and after CE-Chemical reaction was shown in Fig. 2b. The UV-Vis spectra comparison among the original monomer solution (sample D), the reacting solution without FEP (sample E) and with FEP (sample F) were shown in Fig. 2c. The absorption maximum at 370.0 nm and 550.0 nm were only observed in sample F solution, which possibly presented the production of polyaniline and pernigraniline base form of polyaniline due to their π-π * electronic transition [27]. Additionally, some products with brown color (area 1) and white color (area 2) (Fig. 2d(ii)) were deposited on the FEP films (Fig. 2d(i)) after reaction, and their scanning electron microscope (SEM) were shown in Fig. 2d(iii). Fig. 2e showed the Raman spectra of the pristine FEP film, the brown products in area 1 and the white crystals in area 2 on the FEP film. A complex spectrum of the aniline oligomers (AOs) mixture was observed on the brown products in area 1 (red line), showing typical bands of N-phenylphenazinium cation (~1378 cm^{-1}), phenazine-like structure (~1250 cm^{-1} and ~591 cm^{-1}), and linear emeraldine (~1595 cm^{-1}, ~1340 cm^{-1}, ~548 $cm^{-1}$and ~520 cm^{-1}) [28]. The intensity of the peaks at ~1412 cm^{-1} (C~N stretching in a highly localized polaron structure) and ~1448 cm^{-1} (C═N stretching) were connected with the semiquinonoid-charged AOs [29]. The relatively strong intense peaks (white crystals in area 2, blue line) were observed at ~1022 cm^{-1} and ~1004 cm^{-1} that were similar to the typical Raman characteristic peaks of ammonium sulfate [30]. The intense peaks at ~ 732 cm^{-1} and ~384 cm^{-1} in the black line presented the skeleton vibration pattern of the pristine FEP film [14]. From these results, the possible reaction pathway of CE-Polymerization of aniline was inferred in Fig. 2f. Aniline radical cations with different forms were initiated by CE, then two of which might react in a head-to-tail manner to form intermediate or AOs, for further polymerization [31]. .

Radicals as intermediates could not only polymerize monomers through chain growth reaction but also catalyze organic pollutants. As a common organic pollutant in industrial wastewater, phenol is difficult to remove because its chemical scavengers usually cause secondary pollution. Here, a more environmentally friendly degradation way was realized by CE-Chemistry. It can be seen from Figure S14a that the absorption intensity of UV-Vis at 270.0 nm (corresponding to 0.01 mM phenol in DI water) decreased during the CE-Chemical process. It can be also seen from Figure S14b that the oxidation peak (corresponding to the oxide potential at ~ 0.71 V [32]) of phenol disappeared in the CV curve of phenol solution after US in the presence of shredded FEP films for 5 h, which indicated most of the phenol had been oxidized during the CE-Chemical reaction. It was reported that phenol could react with ·OH radicals in (mainly) the ortho-, and some para-, positions to form catechol and hydroquinone, respectively [33]. Further oxidation of the latter compounds then occurred to produce benzoquinones, which would be hydroxylated/oxidized again and ultimately formed lower-molecular-weight acids, carbon dioxide and water [34]. These byproducts may be correlated to the UV-Vis absorption peaks for hydroquinone (~ 300.0 nm), catechol (~ 285.0 nm), p-benzoquinone (~ 254.0 nm), o-benzoquinone (~ 380.0 nm), and carboxylic acids (~ 211.0 nm) [35]. The possible pathways for CE-Catalysis of phenol were shown in figure S14c. The decomposability of reaction products and the recyclability of the sold dielectrics exhibited the CE-Chemical method is a green and effective way to catalyze organic pollutants. In addition, the easy regeneration of the dielectrics could overcome the conventional

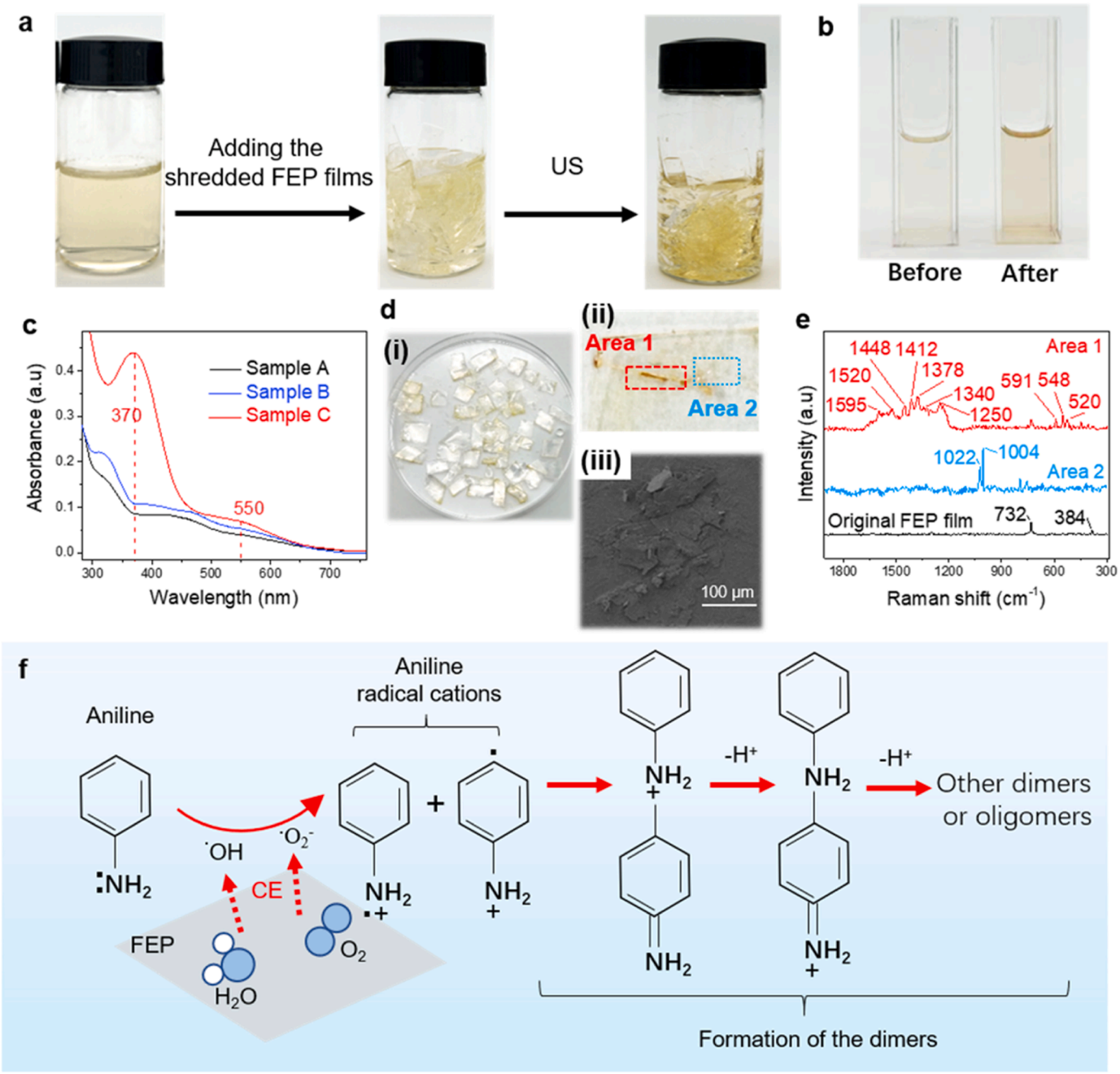

Fig. 2. CE-Chemistry in organic reaction. (a) Photographs of 0.50 M aniline and 0.50 M H_2SO_4 solution under different experimental steps. (b) Photographs of solution sample before and after US in the presence of shredded FEP films (thickness: 30 μm, total area: 600 cm^2) for 10 h. (c) UV-Vis spectra of the solution sample under different conditions, where sample D represented the monomer solution, sample E represented the monomer solution after US, and sample F represented the monomer solution after US in the presence of shredded FEP films. (d) Photographs of the end products, SEM of the end products and (e) Raman spectra of the end products on FEP films. (f) Schematic of aniline polymerization induced by CE.

catalyst poisoning problems.

To investigate the influence of liquid in CE-Chemistry, 0.01 mM phenol was also dissolved into dimethyl sulfoxide (DMSO). It can be seen from Figure S15a(i) that the UV-Vis absorption intensity of 0.01 mM phenol in DMSO at 275.5 nm (Figure S15a(ii)) faded rapidly within the first 5 min of US. Then the UV-Vis absorption intensity at 278.5 nm (Figure S14a(iii)) continued to increase with the increase in US time. This phenomenon was more pronounced with the higher concentration of phenol (1.00 mM) in DMSO solution (Figure S15b). The UV-Vis absorption intensity at 278.5 nm during US might be mainly originated from the oxidation of DMSO itself, as Figure S15c showed the identical UV-Vis absorption from pure DMSO containing FEP but w/o phenol. The UV-Vis absorption peak at 256.5 nm might be due to the generation of some radicals during the oxidation process of DMSO [36], and its intensity decreased quickly within minutes indicated its rapid annihilation, accompanied with an increase in another UV-Vis absorption peak at 278.5 nm (Figure S16a). These radicals were further confirmed as $\cdot O_2^-$ radicals by EPR using DMPO as the radical capture agent as shown in Figure S16b. The intensity of DMPO-$\cdot O_2^-$ in DMSO with FEP was stronger than that in pure DMSO, which demonstrated that FEP greatly promoted the oxidation of DMSO. It was reported that the O_2 in the DMSO was easily to be reduced to form the $\cdot O_2^-$ radicals, because the oxygen atom of DMSO had a lone pair of electrons and could easily lose electrons to O_2 [37]. The introduction of FEP might help O_2 to obtain

more electrons, because the interfacial transferred electron from DMSO to FEP could be more easily captured by O_2 w/o the ionic screening effect of EDL in the organic system. Furthermore, the $\cdot O_2^-$ radicals in solution could oxide phenol, while the unstable DMSO that lost electrons might be further reacted to form other derivatives, such as dimethyl sulfone ($DMSO_2$), SO_2, CH_3SO_3H, and methanesulfinic acid ($CH_3S(O)OH$), etc [37]. FEP is a dielectric material with the electron-accepting capability in the triboelectric series, and DMSO is an organic solvent with the electron-donating capability, which are in line with their electron transfer law during CE (Figure S17). This interesting phenomenon is similar to the century-old generalized Lewis theory that divided chemical compounds into acid/base by their electron pair accepting/donating capability and is widely applied in chemical synthesis. Analogous to the chemical compounds in the generalized Lewis theory, solid dielectrics in CE-Chemistry provided a new paradigm to guide traditional chemical synthesis.

2.3. The influence of EDL formation in CE-chemistry

EDL is a common structure in physiochemistry when studying the solid-liquid interface, but its formation mechanism is still unclear, especially for the EDL formation of insulating solid-liquid interface. One possible explanation of EDL formation was based on the electron transfer during CE between the insulating solid and liquid, followed by the ion absorption on the charged surface of the insulating solid. Herein, the "two-step" EDL model for insulating solid-liquid interface was discussed to show its remarkable effect on the CE-Chemistry. Fig. 3a showed the trend of output charge of SE-TENG, which reflected the

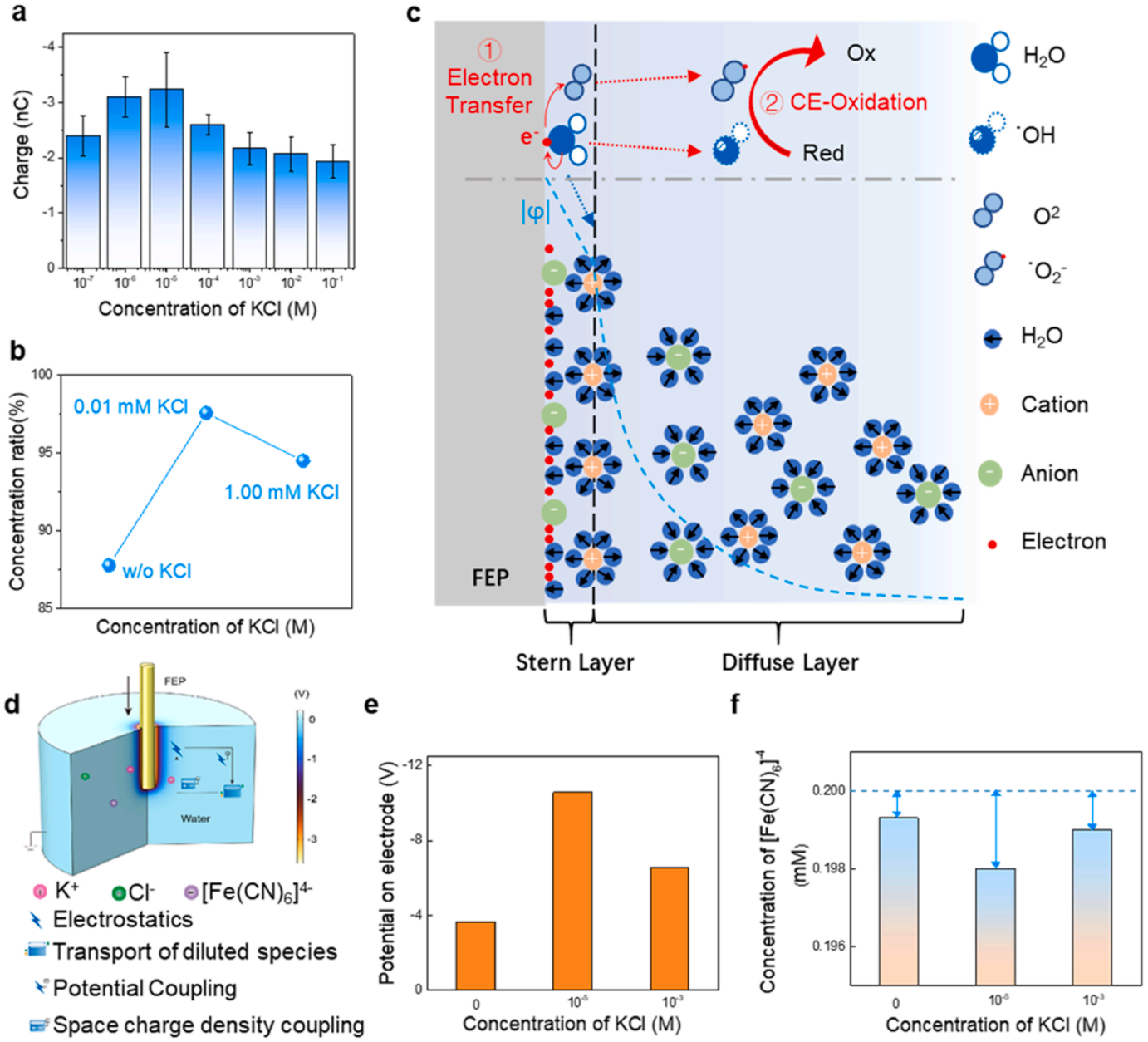

Fig. 3. The influence of EDL formation in CE-Chemistry. (a) Measured charge output trend of SE-TENG in different concentrations of KCl solution. (b) Concentration ratio of products in solution samples with different concentrations of KCl. (c) Schematic of CE-Chemistry in electron transfer and EDL formation. (d) The theoretical model that illustrated the changes in potentials and ion concentrations under different situations. (d) The boundary conditions of theoretical model. (e) The calculated the FEP surface potential and (f) the ion concentrations of $[Fe(CN)_6]^{4-}$, the blue arrows presented the amount of reduced $[Fe(CN)_6]^{4-}$ ions that were oxidized during CE-Chemical reaction.

influence of ion concentration on the interfacial electron transfer between insulating solid dielectrics and liquids. The optimized ion concentration (e.g. 0.01 mM) could enhance ion migration at the FEP-DI water interface during CE, however, a relatively higher (e.g. 0.1 M) ion concentration could excessively inhibit electron transfer due to the screening effect of EDL formation [18]. In CE-Chemistry, the highest concentration of oxidative products ($K_3[Fe(CN)_6]$) was also produced by the optimized ion concentration of 0.01 mM KCl in the reduced $K_4[Fe(CN)_6]$ solution (Fig. 3b). Here, we proposed the relationship of electronic-ionic transfer in the chemical reaction process and EDL formation, as shown in Fig. 3c. During CE at the solid dielectric-liquid interface, electrons were transferred from water to the FEP surface resulting in the negatively charged FEP surface and the generation of hydronium cations and ·OH radicals. The electron might be captures by O_2 to generate $\cdot O_2^-$ radicals induced the CE-Oxidation reaction with ·OH radicals in the diffusion layer. On the other hand, the electron accumulated on the FEP film might adsorb hydronium cations in the vicinity of the solid surface forming the Stern layer. The EDL formation could not only inhibit the further interfacial electron transfer between FEP and water, but also hinder O_2 capturing electrons from the charged FEP surface. To further understand the influence of ionic concertation on CE-Chemistry, the Finite Element Analysis (FEA) and COMSOL modeling were used to simulate the change of surface potential of FEP and EDL formation under various conditions. The theoretical model was depicted in Fig. 3d, the FEP dielectric was immersed into a solution containing $K_4[Fe(CN)_6]$ and KCl, the FEP surface was negatively charged by CE and some anions and cations in the solution were redistributed at the FEP-water interface. The electric field and redistribution of ions at the FEP-solution interface were modeled by the module of electrostatics and transport of diluted species, respectively. The electrostatic potential would affect the movement of solvated ions through potential coupling, meanwhile the redistribution of anions and cations could cause changes in the internal potential of the solution through coupling space charge density. The relationship between potential and ion concentration could be described by the following theoretical formulas:

The ion flux was described by the Nernst-Planck equation [38]:

$$J_i = -D_i\nabla c_i - u_i z_i F c_i \nabla\phi \quad (1)$$

where D_i was diffusion coefficient, c_i was ion concentration, u_i was ionic mobility, z_i was the charge amount of ion, F was Faraday constant, and ϕ was the potential of the solution.

When no further reactions occurred in the solution, the substances obeyed the law of mass conservation:

$$\nabla\cdot J_i = 0 \quad (2)$$

and the electrical potential satisfied the Poisson's equation:

$$\nabla\cdot(-\varepsilon_0\varepsilon_r\nabla\phi) = \rho \quad (3)$$

where ε_0 was vacuum permittivity , ε_r was the relative permittivity of the solution , ρ was the charge density of the solution that can be described as follows:

$$\rho = F\sum_i z_i c_i \quad (4)$$

Additionally, the geometric physical mode was established by the method of 2D-axisymmetric due to its symmetry property. Following the Gouy-Chapman theory, which indicated that the spatial scale of the diffusion layer could be described as the Debye length (x_D) as followed [38,39],

$$x_D = \sqrt{\frac{kT\varepsilon_0\varepsilon_r N_A}{2F^2 c_{bulk}}} \quad (5)$$

where k was the Boltzmann constant , T was the temperature of the solution , N_A was the Avogadro constant , c_{bulk} was the bulk concentration of the solution. Considering the Stern correction of the Gouy-Chapman theory [40], there was a Stern layer in the region close to the FEP, in which the ions would not diffuse with the concentration gradient. The thickness of this layer was defined as x_S.

This model simulated the change of potential over a range of 15 Debye lengths, and its electrical and concentration boundary conditions were shown in Figure S18. The potential and ion concentrations that were far away from the FEP surface were defined as $\phi = 0$ and $c_i = c_{bluk}$, respectively. The specific preset parameters, such as geometry size, electrical parameter, ion concentration, etc., in this model were shown in Table S1. Fig. 3e and f showed that the optimized potential of the FEP surface and the lowest concentration of $[Fe(CN)_6]^{4-}$ near at Stern layer (corresponding to the condition where more $[Fe(CN)_6]^{4-}$ had been oxidized, presented by the blue arrow) were obtained in the reduced $K_4[Fe(CN)_6]$ solution with 0.01 mM KCl. This is possible because the enhanced electron transfer at the FEP-water interface in the optimized concentration generated more ·OH radicals to induce more $[Fe(CN)_6]^{4-}$ to be oxidized in the CE-Chemistry. The detailed changes in potential and $[Fe(CN)_6]^{4-}$ concentrations in solution with different concentrations of KCl were depicted in Figure S19 a and Figure S19b. To further prove the dominant role of radicals in CE-Chemical reactions, the surface of FEP has been negatively pre-charged by ionizing air with an ionic gun (Milty Zerostat 3). Most of the free electrons generated by air ionization could be captured by O_2 to form $\cdot O_2^-$ radicals, these radicals on the pre-charged FEP were transferred in solution could promote the production of oxidized $K_3[Fe(CN)_6]$, compared with that in the original FEP (Figure S20). Therefore, it is important to formulate the CE reactive aqueous solution with optimized ion concentration to avoid the screening effect of EDL formation caused by high ion concentration. In other words, the optimized ion concentration solution could facilitate chemical reactions due to the uppermost charge transfer between solid dielectrics and liquids. It should be noted that in the electrochemical chronocoulometry (CC) method, the cumulative charge of electrode passed in reducing or oxidizing the diffusing reactant could be described by the Anson equation [41], in which the charge transferred is directly correlated to chemical reaction kinetics. In CE-Chemistry, the cumulative charge of solid dielectric (Q_{CE}) is closely related to electronegativity of solid dielectrics, effective contact efficiency of interface, ion concentration etc. The Q_{CE} is analogical to the charge transferred in Anson equation that could determine the chemical reaction kinetics of radical generation and could be regarded as a mean of steering the CE-Chemistry process.

2.4. Steering chemistry by CE

CE-Chemistry is originated from the CE between solid dielectrics and liquids, thus the accepting/donating electron capability of dielectrics at S-L interface may influence the CE-Chemical reactions [42,43], which might be served as a scheme for steering chemical reactions. Taking FEP and polyamide (PA) as an example, where FEP is a typical electron-accepting dielectric, while PA is a typical electron-donating dielectric. In CE-Chemistry, FEP could facilitate the CE-Oxidation of $[Fe(CN)_6]^{4-}$ to $[Fe(CN)_6]^{3-}$, but could not achieve the CE-Reduction of $[Fe(CN)_6]^{3-}$ to $[Fe(CN)_6]^{4-}$ (Figure S21), which indicated the potential applications on using the electronegativity of various solid dielectrics to steer CE-Chemical reactions. Different from FEP, the electron-donating capability of PA could realize the CE-Reduction of $[Fe(CN)_6]^{3-}$ to $[Fe(CN)_6]^{4-}$. As shown in Fig. 4a, the DI water droplet was negatively charged after contacting with PA, which indicated the electrons were transferred from the PA surface to the DI water. As depicted in Fig. 4b, the color of the solution (0.20 mM $K_3[Fe(CN)_6]$ and 0.01 mM KCl) gradually faded after US for 2 h with the shredded PA films. The UV-Vis absorption intensity (at 420.0 nm) of the oxidized $K_3[Fe(CN)_6]$ decreased as the increase in US time (Fig. 4c). An oxidation current peak appeared in the first CV scan for the oxidized $K_3[Fe(CN)_6]$ solution after US in the presence of shredded PA films, while it was not observed in

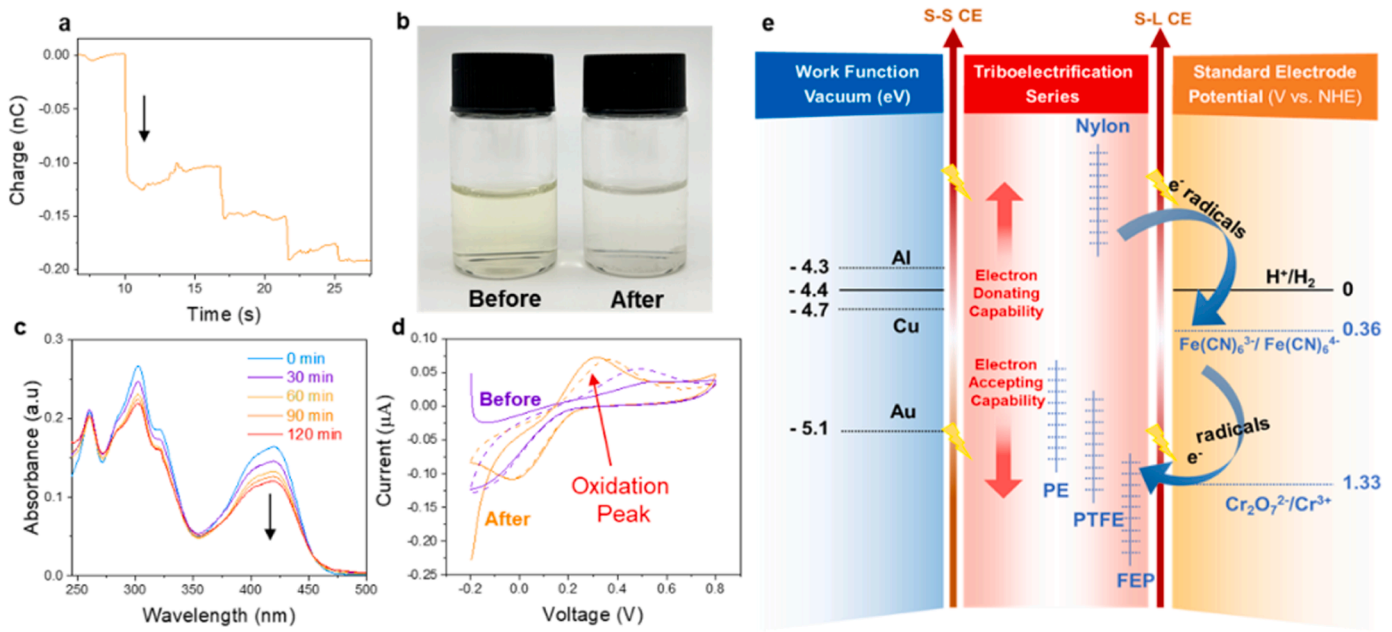

Fig. 4. Steering chemistry by CE. (a) The signal output of DI water droplets after contacting with PA film. (b) Photograph of 0.20 mM $K_3[Fe(CN)_6]$ and 0.01 mM KCl solution before and after US with the shredded PA films (thickness: 30 μm, total area: 600 cm^2). (c) UV-Vis spectra of oxidized $K_3[Fe(CN)_6]$ solution under US in the presence of shredded PA films for 2 h. (d) CV scan curve (scan rate: 1 mV/s) of solution before (purple line) and after (orange line) US with the shredded PA films, the solid and dashed lines were the first and second CV scan cycle, respectively. (e) A guidance that unified the concept of work functions, triboelectric series, and standard electrode potentials by electron transfer capability.

solution before US. This indicated that the CE-Reduction of $[Fe(CN)_6]^{3-}$ to $[Fe(CN)_6]^{4-}$ took place at the PA-water interface (Fig. 4d). After US for 120 min the absorption intensity of the oxidized $K_3[Fe(CN)_6]$ decreased slowly, which showed the CE-Reduction reached the maximum level. This is probably because the rapidly formed EDL resulting in less electron transfer at PA-water interface due to the hydrophilic property of PA (contact angle: 58.44°, Figure S22). When the concentration is low (0.05 mM $K_3[Fe(CN)_6]$), it could be mostly reduced (Figure S23). Moreover, the potassium dichromate ion ($K_2Cr_2O_7^-$) was also observed to be reduced by PA, as its UV-Vis absorption peak at ~ 275.0 nm and ~ 371.0 nm [44] decreased after US in the presence of PA (Figure S24) for 2 h.

The different chemical reactions caused by PA (CE-Reduction) and FEP (CE-Oxidation) in contact with DI water demonstrated that the electronegativity of various dielectrics might be closely related to CE-Chemistry. For example, different results were observed during CE-Oxidation of $K_4[Fe(CN)_6]$ solution with a PTFE stir bar and a glass stir bar. As shown in figure S25, the color of original solution changed from transparent to light green in the presence of the PTFE stir bar, but nothing changed in the presence of the glass stir bar. Moreover, some research mentioned that the fresh PTFE stir bar was detrimental to the synthesis of porphyrin nanorings by reacting with lithium metal, while the glass-coated stir bar did not contribute to side reactions [45]. The reaction of the PTFE stir bar in highly reductive conditions had been indeed observed with metals such as sodium, lithium and even magnesium under the Birch conditions [46]. Brecht *et al.* suggested that, unless exposed to oxygen, a foil of PTFE exposed to sodium in liquid ammonia could contain carbon radicals [47]. All these results implied that the important role of electronegativity of dielectrics in chemical reactions. The relevance of standard electrode potential and work function could be estimated [48], as depicted in Fig. 4e, the "absolute potential" of hydrogen electrode (NHE) at 298.15 K was ~ −4.44 eV. Furthermore, Fig. 4e connected the correlation among the electronegativity of solid dielectrics in triboelectric series, the work function, and the electrochemical redox standard potential by CE. Such scheme provided a guideline to steer CE-Chemical process for the desired reaction products. Additionally, an appropriate ion concentration was important to balance between the mass diffusion and EDL screen effect to optimize CE-Chemistry. Besides, it is beneficial to promote the CE-Chemistry through increasing contact area, prolonging reaction time etc. in practical applications.

3. Conclusion

In this paper, CE-Chemistry as a new paradigm of chemistry, was proved to exist ubiquitously in a wide variety of reactions within aqueous/non-aqueous systems and could be tailored in a controlled way. Unlike piezoelectric-catalysis or electrochemistry, which are limited by the choice of piezoelectric or electro-active materials, CE-Chemistry has the advantage of a wide selection of materials, including the inert dielectrics like PTFE, FEP or PE etc. CE-Chemistry proved not only a physical process, but also a physiochemical process including charge transfer, radical generation and consequent chemical reactions. Compared with conventional initiation methods in reactions, CE-Chemistry provided an alternative to steer reactions more precisely due to its tunable electron transfer capability. The trade-off relationship between EDL formation and electron transfer during CE between solid dielectrics and aqueous solution was further studied and theoretically modeled to optimize CE-Chemistry in aqueous systems. In non-aqueous systems, formation of EDL may not be a dominant process and the electron transfer from the CE might induce more radicals. A guidance that unified the concept of work functions, triboelectric series, and standard electrode potentials was developed. In such a scheme, the thermodynamics of some chemical reactions could be engineered by a wide selection of dielectric materials according to their electronegativity in triboelectric series. Defining order parameters by electron transfer capability could not only provide a new way to steer chemical reactions, but also offer a new perspective to develop multidisciplinary subjects across physics, material science, and chemistry.

4. Method

4.1. Chemicals and materials

Fluorinated ethylene propylene film [FEP, Dupont], polytetrafluoroethylene film and powder [PTFE, Dupont], polyamide film [PA, Dupont], polyethylene film [PE, Dupont], tert-butanol [$C_4H_{10}O$, Sinopharm Chemical Reagent Co., Ltd, 98%], p-phthalic acid [$C_8H_6O_4$, Macklin, 99%], sodium phosphate tribasic dodecahydrate [Na_3PO_4, Aladdin, 99%], 2,2,6,6-tetramethyl-4-piperidone [TEMP, Dojindo], 5,5-dimethyl-1-pyrroline N-oxide [DMPO, Dojindo], phenol [C_6H_5OH, Macklin, 99%], aniline [C_6H_7N, Macklin, 99%], sulfuric acid [H_2SO_4, Macklin, 99%], potassium ferricyanide [$K_3[Fe(CN)_6]$, HengXing, Analytical Reagent], potassium ferrocyanide [$K_3[Fe(CN)_6]$, HengXing, Analytical Reagent], potassium chloride [KCl, HengXing, Analytical Reagent], dimethyl sulfoxide [DMSO, Acmec, 99%].

4.2. Sample preparation

A 12.0 mL sample solution containing 0.20 mM $K_4[Fe(CN)_6]$ (or 0.20 mM $K_3[Fe(CN)_6]$) and 0.01 mM KCl was prepared in advance, about the l of 30.0 cm × 30.0 cm solid dielectric film was cut into 1.0 cm × 1.5 cm pieces and then put into the solution sample. An ultrasonic bath (VGT-190D, 40 kHz, 420 W) was used to promote the CE-Chemistry. The temperature in the ultrasonic bath was regulated. The solution of terephthalic acid was prepared by adding 332.4 mg of p-phthalic acid and 760.0 mg of sodium phosphate tribasic dodecahydrate in 200.0 mL DI water. The solution of aniline solution was prepared by adding 0.5 mL aniline monomer into 9.5 mL sulfuric acid solution with concentration of 0.5 M. The phenol solution was prepared by adding 94.0 mg of phenol to 10.0 mL DI water (or DMSO) and diluting it to a concentration of 0.01 mM. The solid dielectrics after reactions were taken out by using plastic tweezers, then dried in an oven at 40 ℃ overnight before analysis. Samples for EPR analysis were prepared with 12.0 mL of DI water (or DMSO) US with FEP fragments about the total size of 30 cm × 30 cm, and 0.5 mL of DMPO was transferred to the solution during US to capture radicals.

4.3. Sample characterization

The electrical performances of TENG were measured by electrometer (Keithley, 6514), and the electrical properties of the DI water droplets were measured by the Faraday cup. The UV-Vis absorptions of the samples were measured by UV-Vis spectrometer in a range of 200.0–600.0 nm. The emission spectra of THA-OH were measured on an Edinburgh Instruments (FLS 980), using $\lambda_{excitation}$= 225.0 nm and $\lambda_{emission}$= 425.0 nm. The Raman spectroscopy analysis was conducted on a LabRam HR evolution (HORIBA, SAS France), using a range from 300 to 2000 cm^{-1}. Electron paramagnetic resonance (EPR) was recorded on a Bruker EMX plus-9.5/12/ P/L. The measurements were conducted in X-Band (9.830243 GHz), with amplitude modulation of 1 G, microwave power of 2 mW, an amplitude modulation frequency of 100 kHz and conversion time of 60.00 ms, and a time constant at 40.96 ms. The theoretical model is established with COMSOL software and the finite element analysis method. The electrochemical measurements were carried out with the electrochemical workstation (Multi Autolab: M204). The chemical states of solid dielectrics before/after the CE-Chemistry were measured by near atmospheric pressure X-ray photoelectron spectrometer (NAP-XPS, SPECS, Germany). Morphologies of aniline oligomers were observed by the scanning electron microscope (SEM SU8020, Hitachi). X-ray diffraction (XRD) patterns of different solid dielectrics were acquired through an advance diffractometer (Bruker-D8, Germany) with a working voltage of 40 kV. The contact angle of the membrane was characterized using a surface tension meter (Dataphysics OCA20, Germany).

Supporting information

Supplementary data associated with this article can be found in the online version.

CRediT authorship contribution statement

Wang Zhong Lin: Writing – review & editing, Funding acquisition, Conceptualization. **Li Xiang:** Methodology, Investigation. **Li Shaoxin:** Writing – original draft, Visualization, Validation, Resources, Methodology, Investigation, Formal analysis, Data curation, Conceptualization. **Wei Di:** Writing – review & editing, Visualization, Validation, Supervision, Methodology, Funding acquisition, Conceptualization. **Peng Puguang:** Methodology, Data curation. **Zhang Zhiwei:** Writing – original draft, Software, Methodology.

Declaration of Competing Interest

The authors declare the following financial interests/personal relationships which may be considered as potential competing interests: Di Wei reports financial support was provided by The Beijing Natural Science Foundation. If there are other authors, they declare that they have no known competing financial interests or personal relationships that could have appeared to influence the work reported in this paper.

Data Availability

Data will be made available on request.

Acknowledgements

This work was supported by the Beijing Natural Science Foundation (Grant No. IS23040). We thanked Feiyao Yang for constructing experimental equipments, Yaowen Ouyang for helping to prepare solutions, Dr. Ziming Wang for assisting to measure the EPR.

Appendix A. Supporting information

Supplementary data associated with this article can be found in the online version at doi:10.1016/j.nanoen.2024.109286.

References

[1.] K. Ra, M. Teimouri, J. Howarter, C. Jafvert, B. Donaldson, A. Whelton, Critical review: surface water and stormwater quality impacts of cured-in-place pipe repairs, J. Am. Water Works Assoc. 110 (2017) 15–32.
[2] D. Woisetschläger, B. Humpl, M. Koncar, M. Siebenhofer, Electrochemical oxidation of wastewater – opportunities and drawbacks, Water Sci. Technol. 68 (2013) 1173–1179.
[3] Y.S. Zholdassov, et al., Acceleration of Diels-Alder reactions by mechanical distortion, Science 380 (2023) 1053–1058.
[4] T. Friščić, C. Mottillo, H.M. Titi, Mechanochemistry for synthesis, Angew. Chem. Int. Ed. 59 (2020) 1018–1029.
[5] V.V. Boldyrev, K. Tkáčová, Mechanochemistry of solids: past, present, and prospects, J. Mater. Synth. Process. 8 (2000) 121–132.
[6] S. Akbulatov, Y. Tian, Z. Huang, T.J. Kucharski, Q.-Z. Yang, R. Boulatov, Experimentally realized mechanochemistry distinct from force-accelerated scission of loaded bonds, Science 357 (2017) 299–303.
[7] Y. Wang, et al., Piezo-catalysis for nondestructive tooth whitening, Nat. Commun. 11 (2020) 1328.
[8] C.-y Liu, A.J. Bard, Electrostatic electrochemistry at insulators, Nat. Mater. 7 (2008) 505–509.
[9] C.-y Liu, A.J. Bard, Chemical redox reactions induced by cryptoelectrons on a PMMA, Surf. J. Am. Chem. Soc. 131 (2009) 6397–6401.
[10] C.-y Liu, A.J. Bard, Electrons on dielectrics and contact electrification, Chem. Phys. Lett. 480 (2009) 145–156.
[11] B. Baytekin, H.T. Baytekin, B.A. Grzybowski, What really drives chemical reactions on contact charged surfaces? J. Am. Chem. Soc. 134 (2012) 7223–7226.
[12] C. Yun, et al., Can static electricity on a conductor drive a redox reaction: contact electrification of au by polydimethylsiloxane, charge inversion in water, and redox reaction, J. Am. Chem. Soc. 140 (2018) 14687–14695.

[13] H. Li, A. Berbille, X. Zhao, Z. Wang, W. Tang, Z.L. Wang, A contact-electro-catalytic cathode recycling method for spent lithium-ion batteries, Nat. Energy 8 (2023) 1137–1144.
[14] Z. Wang, et al., Contact-electro-catalysis for the degradation of organic pollutants using pristine dielectric powders, Nat. Commun. 13 (2022) 130.
[15] J. Zhao, X. Zhang, J. Xu, W. Tang, Z.L. Wang, F.R. Fan, Contact-electro-catalysis for direct synthesis of H_2O_2 under ambient conditions, Angew. Chem. Int. Ed. 62 (2023) e202300604.
[16] K. Kubota, Y. Pang, A. Miura, H. Ito, Redox reactions of small organic molecules using ball milling and piezoelectric materials, Science 366 (2019) 1500–1504.
[17] S. Lin, X. Chen, Z.L. Wang, Contact electrification at the liquid–solid interface, Chem. Rev. 122 (2022) 5209–5232.
[18] S. Lin, L. Xu, A. Chi Wang, Z.L. Wang, Quantifying electron-transfer in liquid-solid contact electrification and the formation of electric double-layer, Nat. Commun. 11 (2020) 399.
[19] X. Zhang, L. Chen, Y. Jiang, W. Lim, S. Soh, Rationalizing the triboelectric series of polymers, Chem. Mater. 31 (2019) 1473–1478.
[20] Z.L. Wang, A. Chi Wang, On the origin of contact-electrification, Mater. Today 30 (2019) 34–51.
[21] W. Lauterborn, T. Kurz, R. Geisler, D. Schanz, O. Lindau, Acoustic cavitation, bubble dynamics and sonoluminescence, Ultrason. Sonochem. 14 (2007) 484–491.
[22] J. Klíma, C. Bernard, C. Degrand, Sonoelectrochemistry: effects of ultrasound on voltammetric measurements at a solid electrode, J. Electroanal. Chem. 367 (1994) 297–300.
[23] R.G. Compton, J.C. Eklund, S.D. Page, T.J. Mason, D.J. Walton, Voltammetry in the presence of ultrasound: mass transport effects, J. Appl. Electrochem 26 (1996) 775–784.
[24] S. Harish, J. Joseph, K.L.N. Phani, Interaction between gold (III) chloride and potassium hexacyanoferrate (II/III)—does it lead to gold analogue of Prussian blue? Electrochim. Acta 56 (2011) 5717–5721.
[25] S. Li, J. Nie, Y. Shi, X. Tao, F. Wang, J. Tian, S. Lin, X. Chen, Z.L. Wang, Contributions of different functional groups to contact electrification of polymers, Adv. Mater. 25 (2020) 2001307.
[26] Y. Nosaka, A.Y. Nosaka, Generation and detection of reactive oxygen species in photocatalysis, Chem. Rev. 117 (2017) 11302–11336.
[27] D. Wei, C. Kvarnström, T. Lindfors, L. Kronberg, R. Sjöholm, A. Ivaska, Electropolymerization mechanism of N-methylaniline, Synth. Met. 156 (2006) 541–548.
[28] G. Ćirić-Marjanović, M. Trchová, J. Stejskal, The chemical oxidative polymerization of aniline in water: Raman spectroscopy, J. Raman Spectrosc. 39 (2008) 1375–1387.
[29] M. Trchová, Z. Morávková, M. Bláha, J. Stejskal, Raman spectroscopy of polyaniline and oligoaniline thin films, Electrochim. Acta 122 (2014) 28–38.
[30] P.L. Anto, R.J. Anto, H.T. Varghese, C.Y. Panicker, D. Philip, A.G. Brolo, FT-IR, FT-Raman and SERS spectra of anilinium sulfate, J. Raman Spectrosc. 40 (2009) 1810–1815.
[31] N. Kumari Jangid, S. Jadoun, N. Kaur, RETRACTED: a review on high-throughput synthesis, deposition of thin films and properties of polyaniline, Eur. Polym. J. 125 (2020) 109485.
[32] T.A. Enache, A.M. Oliveira-Brett, Phenol and para-substituted phenols electrochemical oxidation pathways, Eur. Polym. J. 655 (2011) 9–16.
[33] J. Morales-Roque, M. Carrillo-Cárdenas, N. Jayanthi, J. Cruz, T. Pandiyan, Theoretical and experimental interpretations of phenol oxidation by the hydroxyl radical, J. Mol. Struc-Theochem. 910 (2009) 74–79.
[34] P. Wang, X.F. Bian, Y.X. Li, Catalytic oxidation of phenol in wastewater — a new application of the amorphous $Fe_{78}Si_9B_{13}$ alloy, Sci. Bull. 57 (2012) 8.
[35] Z.-L. Wu, B. Ondruschka, G. Cravotto, Degradation of phenol under combined irradiation of microwaves and ultrasound, Environ. Sci. Technol. 42 (2008) 8083–8087.
[36] M. Hayyan, M.A. Hashim, I.M. AlNashef, Superoxide ion: generation and chemical implications, Chem. Rev. 116 (2016) 3029–3085.
[37] A. Mardyukov, P.R. Schreiner, Atmospherically relevant radicals derived from the oxidation of dimethyl sulfide, Acc. Chem. Res. 51 (2018) 475–483.
[38] D.A. Aikens, Electrochemical methods: fundamentals and applications, J. Chem. Educ. 60 (1983).
[39] J. Garrido, J. Blanco, Séries A et B., Gauthier-Villars, Académie des sciences, Paris, 1966.
[40] O. Stern, Zur theorie der elektrolytischen doppelschicht, Z. für Elektrochem. und Angew. Phys. Chem. 30 (1924) 508–516.
[41] F.C. Anson, Innovations in the study of adsorbed reactants by chronocoulometry, Anal. Chem. 38 (1966) 54–57.
[42] Y.-J. Zhang, J.-J. Chen, G.-X. Huang, W.-W. Li, H.-Q. Yu, M. Elimelech, Distinguishing homogeneous advanced oxidation processes in bulk water from heterogeneous surface reactions in organic oxidation, Proc. Natl. Acad. Sci. U. S. A. 120 (2023) e2302407120.
[43] X. Chen, et al., Hydrocarbon degradation by contact with anoxic water microdroplets, J. Am. Chem. Soc. 145 (2023) 21538–21545.
[44] X. Tu, Z. Hu, X.-S. Chai, Y. Su, Simple and efficient dual-wavelength spectroscopy for the determination of organic matter in sewage sludge from wastewater treatment, RSC Adv. 9 (2019) 12580–12584.
[45] W. Stawski, J.M. Van Raden, C.W. Patrick, P.N. Horton, S.J. Coles, H.L. Anderson, Strained porphyrin tape-cycloparaphenylene hybrid nanorings, Org. Lett. 25 (2023) 378–383.
[46] C.A. de los Reyes, et al., Adverse effect of ptfe stir bars on the covalent functionalization of carbon and boron nitride nanotubes using billups–birch reduction conditions, ACS Omega 4 (2019) 5098–5106.
[47] N. Chakrabarti, J. Jacobus, The chemical reduction of poly(tetrafluoroethylene), Macromolecules 21 (1988) 3011–3014.
[48] S. Trasatti, Work function, electronegativity, and electrochemical behaviour of metals: II. Potentials of zero charge and "electrochemical" work functions, J. Electroanal. Chem. Interfacial Electrochem. 33 (1971) 351–378.

Dr. Shaoxin Li is a post-doctor in the Beijing Institute of Nanoenergy and Nanosystems. She achieved the Ph.D degree from the University of Chinese Academy of Sciences in 2022 and the B.S. degree from the Jiangsu University in 2017. Her research interest is self-powered sensors, energy harvesting, and solid-liquid contact electrification.

Zhiwei Zhang is a Ph.D. student at the University of Chinese Academy of Sciences (UCAS), under the supervision of Prof. Morten Willatzen. He received a bachelor's degree in physics (/acoustics) from Nanjing University (NJU) in 2019. Afterwards, he served as a short-term research assistant at the Southern University of Science and Technology (SUSTech), engaged in industrial research on intelligent manufacturing. Currently, in the PhD program since 2019, he is working on the piezoelectric, piezotronic and piezo-photonic effects of the nanostructures. His research interests also involve the mathematical and physical modelling of complex systems as well as the finite element method.

Puguang Peng achieved the B.S. and M.S. degrees from the Xiangtan University in 2019 and 2022, respectively. He continues pursuing Ph.D. degree in Beijing Institute of Nanoenergy and Nanosystems, Chinese Academy of Sciences. He focuses on the transformation of ions and electrons, with the applications in iontronics, energy technology and intelligent sensing systems

Xiang Li was born in Heilongjiang Province in 1996. He achieved his B.S. degree from the Shenyang University of Technology in 2018, and his M.S. degree from the Shenyang Jianzhu University in 2022. He is studying for the Ph.D. degree at Beijing Institute of Nanoenergy and Nanosystems. His research interest is the triboelectric nanogenerator.

Prof. Zhong Lin Wang received his Ph.D. from Arizona State University in physics. He now is the Hightower Chair in Materials Science and Engineering, Regents' Professor, Engineering Distinguished Professor and Director, Center for Nanostructure Characterization, at Georgia Tech. Dr. Wang has made original and innovative contributions to the synthesis, discovery, characterization and understanding of fundamental physical properties of oxide nanobelts and nanowires, as well as applications of nanowires in energy sciences, electronics, optoelectronics and biological science. His discovery and breakthroughs in developing nanogenerators established the principle and technological road map for harvesting mechanical energy from environment and biological systems for powering personal electronics. His research on self-powered nanosystems has inspired the worldwide effort in academia and industry for studying energy for micro-nano-systems, which is now a distinct disciplinary in energy research and future sensor networks. He coined and pioneered the field of piezotronics and piezophototronics by introducing piezoelectric potential gated charge transport process in fabricating new electronic and optoelectronic devices. Details can be found at: http://www.nanoscience.gatech.edu.

Prof. Di Wei is the principle investigator at BINN, Head of the Flexible Iontronics Laboratory. As the Fellow of the Royal Society of Chemistry (FRSC) and Senior Member of Wolfson College at Cambridge University, he has published over 100 papers including Nature Energy, Nature Commun., PNAS, Adv Mater, Energ Environ Sci., Matter etc. Till end of 2022, more than 160 international patents (including PCT) have been applied, 57 international patents and 27 Chinese patents have been granted. He also edited 3 English books published in Wiley and Cambridge University Press etc. focusing on nanotechnology for energy and sensors. Details can be found at: http://iontronics.group/